Vibrational spectroscopic study of the sulphate mineral glaucocerinite $(Zn,Cu)_{10}Al_6(SO_4)_3(OH)_{32}\cdot 18H_2O$ –a natural layered double hydroxide

Ray L. Frost[a•], Frederick L. Theiss, [a]Andrés López[a], Ricardo Scholz[b]

[a] School of Chemistry, Physics and Mechanical Engineering, Science and Engineering Faculty, Queensland University of Technology, GPO Box 2434, Brisbane Queensland 4001, Australia.

[b] Geology Department, School of Mines, Federal University of Ouro Preto, Campus Morro do Cruzeiro, Ouro Preto, MG, 35,400-00, Brazil.

Abstract:

We have studied the molecular structure of the mineral glaucocerinite $(Zn,Cu)_5Al_3(SO_4)_{1.5}(OH)_{16}\cdot 9(H_2O)$ using a combination of Raman and infrared spectroscopy. The mineral is one of the hydrotalcite supergroup of natural layered double hydroxides. The Raman spectrum is characterised by an intense Raman band at 982 cm^{-1} with a low intensity band at 1083 cm^{-1}. These bands are attributed to the sulphate symmetric and antisymmetric stretching mode. The infrared spectrum is quite broad with a peak at 1020 cm^{-1}. A series of Raman bands at 546, 584, 602, 625 and 651 cm^{-1} are assigned to the $\nu_4 (SO_4)^{2-}$ bending modes. The observation of multiple bands provides evidence for the reduction in symmetry of the sulphate anion from T_d to C_{2v} or even lower symmetry. The Raman band at 762 cm^{-1} is attributed to a hydroxyl deformation mode associated with AlOH units. Vibrational spectroscopy enables aspects of the molecular structure of glaucocerinite to be determined.

Keywords: Raman spectroscopy, glaucocerinite, sulphate, infrared spectroscopy

• Author for correspondence (r.frost@qut.edu.au) P +61 7 3138 2407 F: +61 7 3138 1804

Introduction

Studies of anionic clays have been undertaken for a long time [1-3]. In this work we are undertaking a study of glaucocerinite $(Zn,Cu)_5Al_3(SO_4)_{1.5}(OH)_{16}\cdot 9(H_2O)$. Anionic clays, hydrotalcites or layered double hydroxides (LDH) are less well-known than cationic clays like smectites [4-6]. The structure of hydrotalcite can be derived from a brucite structure ($Mg(OH)_2$) in which e.g. Al^{3+} or Fe^{3+} (pyroaurite-sjögrenite) substitutes a part of the Mg^{2+}. This substitution creates a positive layer charge on the hydroxide layers, which is compensated by interlayer anions or anionic complexes. In hydrotalcites, a broad range of compositions are possible of the type $[M^{2+}_{1-x}M^{3+}_x(OH)_2][A^{n-}]_{x/n}.yH_2O$, where M^{2+} and M^{3+} are the di- and trivalent cations in the octahedral positions within the hydroxide layers with x normally between 0.17 and 0.33. A^{n-} is an exchangeable interlayer anion. Many variations in compositions have been reported for hydrotalcites. In a recent study, Mills et al. [7] have described the hydrotalcite supergroup as the grouping of several mineral groups: hydrotalcite, quintinite, fougèrite, woodwardite, glaucocerinite, wermlandite, cualstibite, hydrocalumite as well as unclassified minerals in a total of 43 approved minerals. In previous studies, the former hydrotalcite group minerals were described as members of manasseite groups of minerals composed by hexagonal carbonates and the triclinic carbonates known as the hydrotalcites or double layer hydroxides [8-11]. In the normal course of events, it is essential to determine the X-ray diffraction of the layered double hydroxide or hydrotalcite like compound. In this was the interlayer space may be determined and the structure ascertained. Single crystal XRD is not normally used as the size of the crystals of the layered double hydroxide or hydrotalcite like compound are too small. For this reason vibrational spectroscopy is essential for the determination of the molecular structure of the mineral.

The mineral glaucocerinite $(Zn,Cu)_5Al_3(SO_4)_{1.5}(OH)_{16}\cdot 9(H_2O)$ is a sulphate based mineral [12] and is one of the hydrotalcite supergroup of natural layered double hydroxides [13]. According to Raade et al., the structure is hexagonal and is related to a pyroaurite-*2H* type structure [12]. The mineral is found in acid mine drainage, old mine sites (such as the old lead mines from Laurion, Greece) [14, 15] and polluted waterways [14, 16, 17]. . According to Raade et al. [12], the alleged co-type glaucocerinite from Laurion is related to woodwardite and has the formula $[(Zn,Cu)_2Al(OH)_6][(SO_4)_{0.5}\cdot 3H_2O]$. This woodwardite-like mineral has a cation-ordered pyroaurite-*2H* structure with hexagonal cell parameters a = 5.306(2) and c = 26.77(2) Å; its strongest X-ray powder lines occur at 8.9 (100)(003), 4.47 (90)(006), 2.55 (60)(113), and 2.28 Å (50)(116). So-called woodwardite from

Caernarvonshire (Wales) is the Cu-analogue of glaucocerinite, whereas an 11-Å mineral occurring with carrboydite in Western Australia is the Ni-analogue. According to Mills et al. [13] glaucocerinite is still an accepted mineral name as is the glaucocerinite group which currently also includes hydrowoodwardite, carrboydeite, hydrohonessite, mountkeithite and zincaluminite (though Mills et al. currently lists carrboydeite and zincaluminite as questionable species). In the past, glaucocerinite phases have been confused with woodwardite, hydrowoodwardite and zincowoodwardite phases [13]. One reason for undertaking the spectroscopic analysis of glaucocerinite is to see if this mineral may be distinguished from the others above.

Spectroscopic methods are the most direct and powerful means of obtaining experimental information on the electronic structure of materials. Moreover, Raman spectroscopy is considered a powerful tool in order to estimate the degree of structural order–disorder at short-range in different types of the materials. Raman spectroscopy has proven most useful for the study of mineral structure. The objective of this research is to report the Raman and infrared spectra of glaucocerinite and to relate the spectra to the mineral structure.

Experimental

Samples description and preparation

The glaucocerinite sample studied in this work forms part of the collection of the Geology Department of the Federal University of Ouro Preto, Minas Gerais, Brazil, with sample code SAA-197. The sample was gently crushed and the associated minerals were removed under a stereomicroscope (Leica MZ4). The glaucocerinite studied in this work occurs as single crystals with prismatic hexagonal form up to 5 mm. The mineral was identified with X-ray diffraction and the unit cell parameters were refined. Scanning electron microscopy (SEM) in the EDS mode was applied to support the mineral characterization. In the normal course of events, we would undertake SEM and EDX analysis. In this way the chemical composition of the mineral may be obtained. The mineral glaucocerinite is quite difficult to handle because of its partial solubility. Thus, these experiments were not undertaken. It was impossible to polish the crystals.

Raman microprobe spectroscopy

Crystals of glaucocerinite were placed on a polished metal surface on the stage of an Olympus BHSM microscope, which is equipped with 10x, 20x, and 50x objectives. The microscope is part of a Renishaw 1000 Raman microscope system, which also includes a monochromator, a filter system and a CCD detector (1024 pixels). The Raman spectra were excited by a Spectra-Physics model 127 He-Ne laser producing highly polarized light at 633 nm and collected at a nominal resolution of 2 cm^{-1} and a precision of ± 1 cm^{-1} in the range between 200 and 4000 cm^{-1}. Repeated acquisitions on the crystals using the highest magnification (50x) were accumulated to improve the signal to noise ratio of the spectra. Raman Spectra were calibrated using the 520.5 cm^{-1} line of a silicon wafer.

Infrared spectroscopy

Infrared spectra were obtained using a Nicolet Nexus 870 FTIR spectrometer with a smart endurance single bounce diamond ATR cell. Spectra over the 4000–525 cm^{-1} range were obtained by the co-addition of 128 scans with a resolution of 4 cm^{-1} and a mirror velocity of 0.6329 cm/s. Spectra were co-added to improve the signal to noise ratio.

Spectral manipulation such as baseline correction/adjustment and smoothing were performed using the Spectracalc software package GRAMS (Galactic Industries Corporation, NH, USA). Band component analysis was undertaken using the Jandel 'Peakfit' software package that enabled the type of fitting function to be selected and allows specific parameters to be fixed or varied accordingly. Band fitting was done using a Lorentzian-Gaussian cross-product function with the minimum number of component bands used for the fitting process. The Gaussian-Lorentzian ratio was maintained at values greater than 0.7 and fitting was undertaken until reproducible results were obtained with squared correlations of r^2 greater than 0.995.

Results and discussion

Vibrational Spectroscopy

Background

The Raman spectroscopy of the aqueous sulphate tetrahedral oxyanion yields the symmetric stretching (ν_1) vibration at 981 cm^{-1}, the in-plane bending (ν_2) mode at 451 cm^{-1}, the antisymmetric stretching (ν_3) mode at 1104 cm^{-1} and the out-of-plane bending (ν_4) mode

at 613 cm^{-1} [18]. Ross [19, 20] reports the interpretation of the infrared spectra for potassium alum as ν_1, 981 cm^{-1}; ν_2, 465 cm^{-1}; ν_3, 1200, 1105 cm^{-1}; ν_4, 618 and 600 cm^{-1} [19]. Water stretching modes were reported at 3400 and 3000 cm^{-1}, bending modes at 1645 cm^{-1}, and librational modes at 930 and 700 cm^{-1} [20]. The Raman spectrum of the mineral chalcanthite shows a single symmetric stretching mode at 984.7 cm^{-1}. Two ν_2 modes are observed at 463 and 445 cm^{-1} and three ν_3 modes at 1173, 1146 and 1100 cm^{-1}. The ν_4 mode is observed as a single band at 610 cm^{-1}. A complex set of overlapping bands is observed in the low wavenumber region at 257, 244, 210 136 and 126 cm^{-1}. Recently, Raman spectra of four basic copper sulphate minerals, namely antlerite, brochiantite, posnjakite and langite, were published [21]. The SO symmetric stretching modes for the four basic copper sulphate minerals are observed at 985, 990, 972 and 974 cm^{-1} respectively. Only the mineral brochantite showed a single band in this region. Multiple bands were observed for these minerals in the antisymmetric stretching region.

Ross [19] also lists the infrared spectra of the pseudo-alums formed from one divalent and one trivalent cations. Halotrichite has infrared bands at ν_1, 1000 cm^{-1}; ν_2, 480 cm^{-1}; ν_3, 1121, 1085, 1068 cm^{-1}; ν_4, 645, 600 cm^{-1}. Pickeringite the Mg end member of the halotrichite-pickeringite series has infrared bands at ν_1, 1000 cm^{-1}; ν_2, 435 cm^{-1}; ν_3, 1085, 1025 cm^{-1}; ν_4, 638, 600 cm^{-1} [19]. These minerals display infrared water bands in the OH stretching, 3400 and 3000 cm^{-1} region; OH deformation, 1650 cm^{-1} region; OH libration, 725 cm^{-1} region. Ross also reports a weak band at ~960 cm^{-1} which is assigned to a second OH librational vibration [19]. As with the infrared spectra, Raman spectra of alums are based on the combination of the spectra of the sulphate and water. Sulphate typically is a tetrahedral oxyanion with Raman bands at 981 (ν_1), 451 (ν_2), 1104 (ν_3) and 613 (ν_4) cm^{-1}[22]. Some sulphates have their symmetry reduced through acting as monodentate and bidentate ligands [22]. In the case of bidentate behaviour both bridging and chelating ligands are known. This reduction in symmetry is observed by the splitting of the ν_3 and ν_4 into two components under C_{3v} symmetry and 3 components under C_{2v} symmetry.

Vibrational spectroscopy

The Raman spectrum of glaucocerinite over the complete measured wavenumber range is displayed in Figure 1a. This figure shows the position of the Raman bands and their relative intensities and also provides an indication of the sharpness of these bands. Large parts of the

spectrum are noted where little or no intensity is found. Therefore, the spectra are subdivided into sections based upon the differing vibrations being studied. The infrared spectrum of glaucocerinite over the 500 to 4000 cm^{-1} spectral range is reported in Figure 1b. This figure shows the position and relative intensities of the infrared active glaucocerinite bands. The spectra are subdivided into sections as is convenient, based upon the vibrations being studied.

The Raman spectrum of glaucocerinite over the 800 to 1400 cm^{-1} spectral range is displayed in Figure 2a. This spectral region is the region of the symmetric stretching modes. The spectrum is dominated by an intense Raman band at 991 cm^{-1}. The position of this band is in agreement with previously published data [23].Two low intensity shoulders to this band are observed at 982 and 998 cm^{-1}. This band at 999 cm^{-1} is assigned to the SO_4^{2-} ν_1 symmetric stretching mode. In addition, Raman bands are observed at 1072 (sharp), 1118 (very broad) and 1206 cm^{-1}. These bands with the exception of the 1072 cm^{-1} band may be attributed to the SO_4^{2-} ν_3 antisymmetric stretching mode.

A comparison of the spectra of glaucocerinite may be made with other sulphate containing minerals. Natural carrboydite is characterised by an intense band centred at 980 cm^{-1} and is assigned to the SO_4^{2-} symmetric stretching vibration. A very broad band for natural carrboydite is observed at around 1125 cm^{-1} and this must be the observation of the Raman bands of the SO_4^{2-} antisymmetric stretching vibrations. The infrared spectrum of carrboydite shows three bands at 1088, 1021 and 978 cm^{-1}. The first two bands are due to the intense SO_4^{2-} antisymmetric stretching vibrations and the last band is the weak infrared SO_4^{2-} symmetric stretching vibration. No carbonate bands at around 1060 cm^{-1} was observed in the Raman spectrum; thus indicating the carrboydite was a pure sulphate mineral with no carbonate exchange. In contrast, the Raman spectrum of both hydrohonessite and reevesite show sharp bands at 1008 cm^{-1}. Hydrohonessite Raman spectrum shows two bands at 1135 and 1115 cm^{-1}. The reevesite Raman spectrum displays two bands at 1135 and 1118 cm^{-1}. The infrared spectrum of hydrohonessite shows two intense bands at 1088 and 1021 cm^{-1}. A very weak band is observed at 978 cm^{-1}. In comparison the bandwidths of the infrared peaks are very broad. The Raman spectrum of mountkeithite displays two bands at 1129 and 1109 cm^{-1}, assigned to the SO_4^{2-} antisymmetric stretching vibrations.

According to Myneni [24], the SO_4^{2-} polyhedra of the channels in glaucocerinite are present in three crystallographically different sites and exhibit weakly split S-O antisymmetric stretching vibrations at 1136 cm^{-1} (with several components) and symmetric stretch at 1016, 1008, and 989 cm^{-1}. The observation of three symmetric stretching bands in this work, fits well with the concept of three different non-equivalent sulphate units in the glaucocerinite structure. These researchers [24] studied the incorporation of arsenate ions into the glaucocerinite structure and reported the changes in the Raman and infrared spectra during this adsorption. The band at 1072 cm^{-1} looks very much like a carbonate stretching mode. It is possible that the mineral being studied is a solid solution of glaucocerinite. Thus the presence of this latter mineral in the solid solution would give rise to the carbonate bands.

Bish and Livingstone observed for honessite the sulphate ν_1, ν_2, ν_3 and ν_4 modes at 980, 500, 1140 and 650 cm^{-1}, respectively [25]. The ν_3 mode is clearly split but no separate band positions were given. The infrared spectrum of synthetic hydrohonessite was very similar to that of the naturally occurring honessite [25]. Although the split of the ν_3 mode is only visible as a weak shoulder on the low wavenumber side of the comparatively broad band in contrast to the (hydro)honessite, where the weaker of the two bands is observed as a separate band or shoulder at the higher wavenumber side. The fact that these authors found all four modes to be infrared active indicates that the symmetry of the sulphate anion has been lowered from T_d for the free anion to C_3 or C_{3v}, which would result in activation of the two infrared inactive modes plus splitting of the ν_3 mode. Dutta and Puri observed bands associated with the sulphate anion in Li/Al-hydrotalcite in the Raman spectrum around 457, 467, 620 (all three weak), 986 and 1116 cm^{-1} (broad). The splitting of ν_2 and the broadening of the antisymmetric stretching mode ν_3 indicate a significant symmetry lowering. Dutta and Puri [26] suggested D_2 which is however not compatible with the infrared data where all four bands have been observed [26]. For similar reasons C_3 site symmetry as suggested by Bish is not compatible with the Raman data. Therefore, based on combined observations in both the infrared and Raman spectra the conclusion has to be that the site symmetry is most probably C_{2v} or C_s with ν_1 A_1 infrared and Raman active, ν_2 A_1 infrared and Raman active, ν_2 A_2 only Raman active, and ν_3 and ν_4 $A_1 + B_1 + B_2$ all infrared and Raman active. The infrared spectrum over the 900 to 1100 cm^{-1} spectral range is shown in Figure 2b. Strong infrared bands are observed at 1053, 1078 and 1109 cm^{-1} which may be assigned to the SO_4^{2-} ν_3

antisymmetric stretching mode. The low intensity infrared band at 986 cm^{-1} is attributed to the SO_4^{2-} ν_1 symmetric stretching mode.

The Raman spectra of glaucocerinite over the 300 to 800 cm^{-1} spectral range and over the 100 to 300 cm^{-1} spectral range are shown in Figure 3. A series of Raman bands are observed at 546, 584, 602, 625 and 651 cm^{-1}. These bands are assigned to the ν_4 $(SO_4)^{2-}$ bending modes. Renaudin et al. [23] found a Raman band at 549 cm^{-1} for a synthetic glaucocerinite analogue and attributed this band to an $Al(OH)_6$ vibration. We found a Raman band at 546 cm^{-1}. The observation of multiple bands in this ν_4 spectral region offers evidence for the reduction in symmetry of the sulphate anion from T_d to C_{2v} or even lower symmetry. The Raman band at 762 cm^{-1} is attributed to a hydroxyl deformation mode associated with AlOH units. It is likely that the infrared bands at 851 and 877 cm^{-1} are also due to this vibrational unit. The Raman band at 455 cm^{-1} with a low wavenumber shoulder at 430 cm^{-1} are ascribed to the ν_2 $(SO_4)^{2-}$ bending modes. Renaudin et al. [23] found a band at 451 cm^{-1} for a synthetic glaucocerinite analogue and assigned this band to a ν_2 sulphate vibration. The band at 359 cm^{-1} is attributed to a CaO stretching vibration. In the far low wavenumber region a broad spectral feature is observed which may be resolved into component bands at 115, 180, 211 and 237 cm^{-1}. These bands are simply described as lattice vibrations.

The Raman spectrum of glaucocerinite over the 3000 to 3800 cm^{-1} spectral range is illustrated in Figure 4a. The spectrum shows two features: a band at 3629 cm^{-1} and a broad feature at around 3500 cm^{-1}. This latter band may be resolved into component bands at 3260, 3386 and 3487 cm^{-1}. The first band at 3629 cm^{-1} is assigned to the OH stretching vibration of the OH units. The broad feature is attributed to water stretching vibrations. Renaudin et al. observed the OH stretching vibration at 3638 cm^{-1}. These researchers found the water band at 3440 cm^{-1} and found the band was very broad. The infrared spectrum of glaucocerinite over the 2600 to 3800 cm^{-1} spectral range is shown in Figure 4b. The spectral profile of the infrared spectrum resembles the Raman spectrum in this spectral region. An infrared band is found at 3626 cm^{-1} assigned to the OH stretching vibration of the OH units. The broad band centred upon 3398 cm^{-1} is assigned to water stretching vibration. The broad band may be resolved into component bands at 3116, 3241 and 3398 cm^{-1}. The infrared spectrum of glaucocerinite over the 1300 to 1800 cm^{-1} spectral range is shown in Figure 5. It should be noted no intensity was found over this spectral range in the Raman spectrum. Two infrared bands are

found at 1636 and 1676 cm^{-1} and are assigned to water stretching vibrational modes. The band at 1403 cm^{-1} may be due to a carbonate impurity. Thus, the presence of this latter mineral in the solid solution would give rise to the carbonate bands.

Conclusions

The structure of hydrotalcite-*2H* can be derived from a brucite structure ($Mg(OH)_2$) in which trivalent cations e.g. Al^{3+} or Fe^{3+} (pyroaurite-*2H*) substitutes as part of the Mg^{2+}. This substitution creates a positive layer charge on the hydroxide layers, which is compensated by interlayer anions or anionic complexes.

Water plays a unique role in the stabilisation of the hydrotalcite-*2H* structure. The position and intensity of the Raman bands in the hydroxyl-stretching region indicates that the water is highly structured. The position of the bands in the hydroxyl deformation region of the infrared spectrum supports the concept of structured water between the hydrotalcite layers. Four types of water are identified (a) water hydrogen bonded to the interlayer carbonate ion (b) interlamellar water (c) water hydrogen bonded to the hydroxyl units (d) water which bridges the sulphate anion and the M_3OH surface. The position of the suite of bands associated with the sulphate ion indicates the carbonate ion is perturbed and not bonded to the metal centres but is strongly hydrogen bonded to the interlayer water. An intense band at around 559 cm^{-1} is observed and it is proposed that this band is due to the librational mode of water hydrogen bonded to the metal hydroxyl surface.

In this work, the Raman spectra of the interlayer anions of sulphate of a natural mineral glaucocerinite have been collected. The splitting of the ν_3, ν_4 and ν_2 modes indicates symmetry lowering. The symmetry lowering must be taken into account through the bonding of the sulphate anion to both water and the brucite-like hydroxyl surface. Water plays an essential role in the glaucocerinite -*2H* structure as may be evidenced by the position of the water bending modes. The water is strongly hydrogen bonded to both the anions and the hydroxyl surface. Raman spectroscopy has the advantage that water molecules are not observed as water is a very poor Raman scatterer. Water is however easily measured with infrared spectroscopy. The combination of the two techniques enables the bands ascribed to hydroxyl units and to water molecules to be distinguished. Thus the cation OH stretching vibrations are more readily observed with Raman spectroscopy.

Acknowledgements

The financial and infra-structure support of the Discipline of Nanotechnology and Molecular Science, Science and Engineering Faculty of the Queensland University of Technology, is gratefully acknowledged. The Australian Research Council (ARC) is thanked for funding the instrumentation. The authors would like to acknowledge the Center of Microscopy at the Universidade Federal de Minas Gerais (http://www.microscopia.ufmg.br) for providing the equipment and technical support for experiments involving electron microscopy. R. Scholz thanks to CNPq – Conselho Nacional de Desenvolvimento Científico e Tecnológico (grant No. 306287/2012-9).

References

[1] C. Frondel, American Mineralogist 26 (1941) 295.

[2] M.C. Van Oosterwyck-Gastuche, G. Brown, M.M. Mortland, Clay Minerals 7 (1967) 177.

[3] C.W. Beck, American Mineralogist 35 (1950) 985.

[4] J.T. Kloprogge, D. Wharton, L. Hickey, R.L. Frost, American Mineralogist 87 (2002) 623.

[5] R.L. Frost, W.N. Martens, L. Duong, J.T. Kloprogge, Journal of Materials Science Letters 21 (2002) 1237.

[6] L. Hickey, J.T. Kloprogge, R.L. Frost, Journal of Materials Science 35 (2000) 4347.

[7] S.J. Mills, A.G. Christy, J.M.R. Genin, T. Kameda, F. Colombo, Mineralogical Magazine 76 (2012) 1289.

[8] A.S. Bookin, V.I. Cherkashin, V.A. Drits, Clays and Clay Minerals 41 (1993) 558.

[9] V.A. Drits, N.A. Lisitsyna, V.I. Cherkashin, Doklady Akademii Nauk SSSR 284 (1985) 443.

[10] V.A. Drits, T.N. Sokolova, G.V. Sokolova, V.I. Cherkashin, Izvestiya Akademii Nauk SSSR, Seriya Geologicheskaya (1986) 76.

[11] V.A. Drits, T.N. Sokolova, G.V. Sokolova, V.I. Cherkashin, Clays and Clay Minerals 35 (1987) 401.

[12] G. Raade, C.J. Elliott, V.K. Din, Mineralogical Magazine 49 (1985) 583.

[13] S.J. Mills, A.G. Christy, J.M.R. Genin, T. Kameda, F. Colombo, Mineralogical Magazine 76 (2012) 1289.

[14] P. Schreck, T. Witzke, H. Pollmann, Applied Mineralogy: In Research, Economy, Technology, Ecology and Culture, Proceedings of the International Congress on Applied Mineralogy, 6th, Goettingen, Germany, July 17-19, 2 2 (2000) 679.

[15] M. Schubert, R. Wennrich, H. Weiss, P. Schreck, T. Zeller, H.H. Otto, H. Wolfram, European Journal of Mineralogy 17 (2005) 119.

[16] J.J. Kim, Y.H. Kim, S.W. Choi, Y.D. Jang, C.S. Yu, E.S. Woo, Abstracts of Papers, 239th ACS National Meeting, San Francisco, CA, United States, March 21-25, 2010 (2010) GEOC.

[17] E.S. Woo, J.J. Kim, Y.H. Kim, G.C. Jeong, Y.D. Jang, W.A. Dick, Environmental Earth Sciences 69 (2013) 2199.

[18] R.L. Frost, P.A. Williams, W. Martens, J.T. Kloprogge, P. Leverett, Journal of Raman Spectroscopy 33 (2002) 260.

[19] S.D. Ross, in The infrared spectra of minerals, Chapter 18 pp 423 (1974) The Mineralogical Society London.

[20] S.D. Ross, Inorganic Infrared and Raman Spectra (European Chemistry Series). 1972.

[21] W. Martens, R.L. Frost, J.T. Kloprogge, P.A. Williams, Journal of Raman Spectroscopy 34 (2003) 145.

[22] R.L. Frost, J.T. Kloprogge, P.A. Williams, P. Leverett, Journal of Raman Spectroscopy 31 (2000) 1083.

[23] G. Renaudin, R. Segni, D. Mentel, J.-M. Nedelec, F. Leroux, C. Taviot-Gueho, Journal of Advanced Concrete Technology 5 (2007) 299.

[24] S.C.B. Myneni, S.J. Traina, G.A. Waychunas, T.J. Logan, Geochimica et Cosmochimica Acta 62 (1998) 3499.

[25] D.L. Bish, A. Livingstone, Mineralogical Magazine 44 (1981) 339.

[26] P.K. Dutta, M. Puri, Journal of Physical Chemistry 93 (1989) 376.

List of Figures

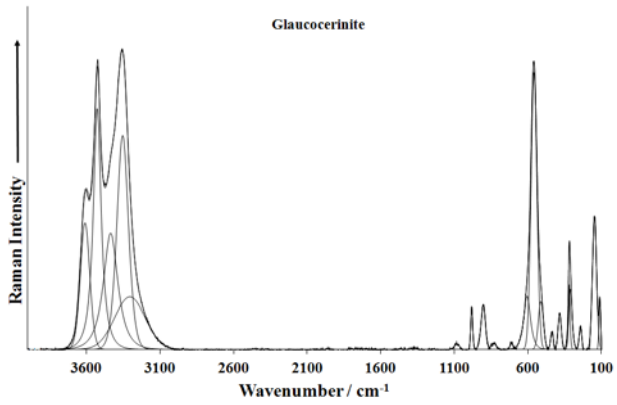

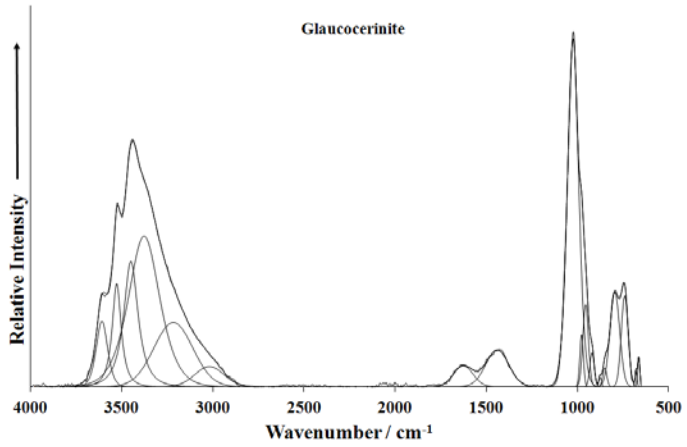

Figure 1a Raman spectrum of glaucocerinite (upper spectrum) over the 100 to 4000 cm^{-1} spectral range and Figure 1b infrared spectrum of glaucocerinite (lower spectrum) over the 500 to 4000 cm^{-1} spectral range

394

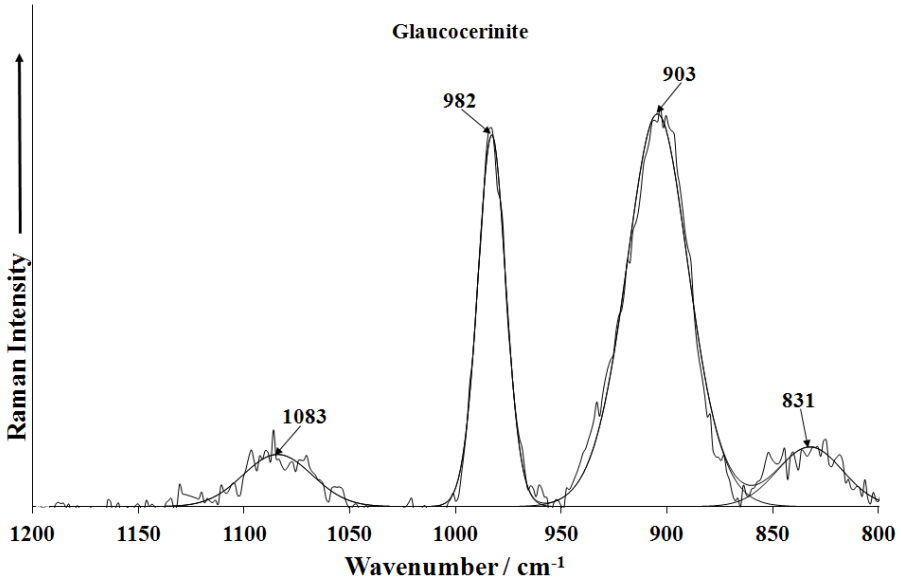

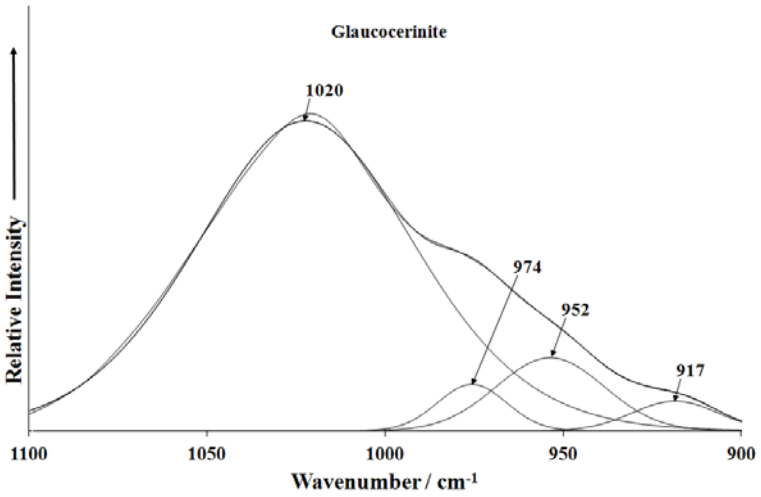

Figure 2a Raman spectrum of glaucocerinite (upper spectrum) in the 800 to 1200 cm^{-1} spectral range and Figure 2b infrared spectrum of glaucocerinite (lower spectrum) in the 900 to 1100 cm^{-1} spectral range

395

396

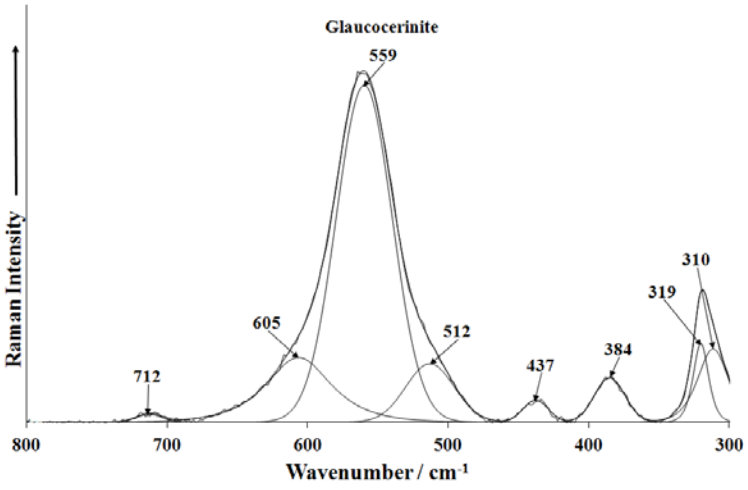

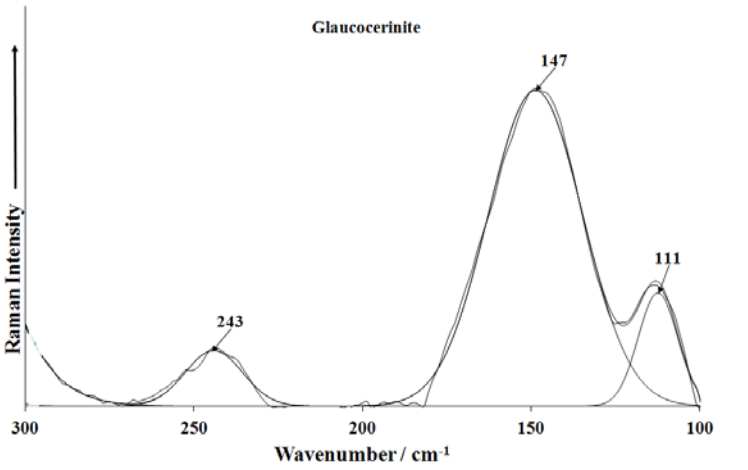

Figure 3a Raman spectrum of glaucocerinite (upper spectrum) in the 300 to 800 cm^{-1} spectral range and Figure 3b Raman spectrum of glaucocerinite (lower spectrum) in the 100 to 300 cm^{-1} spectral range

397

398

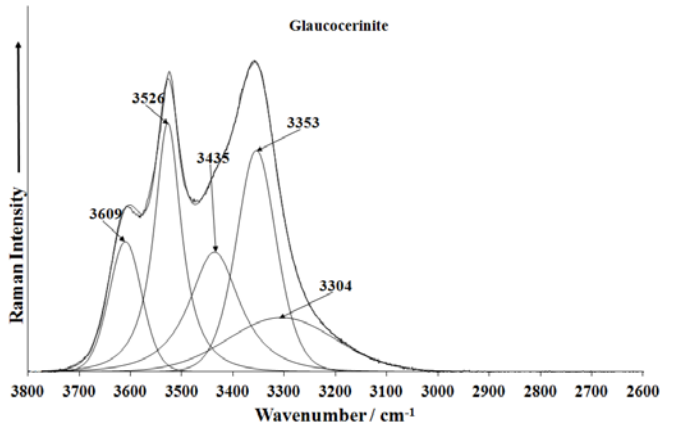

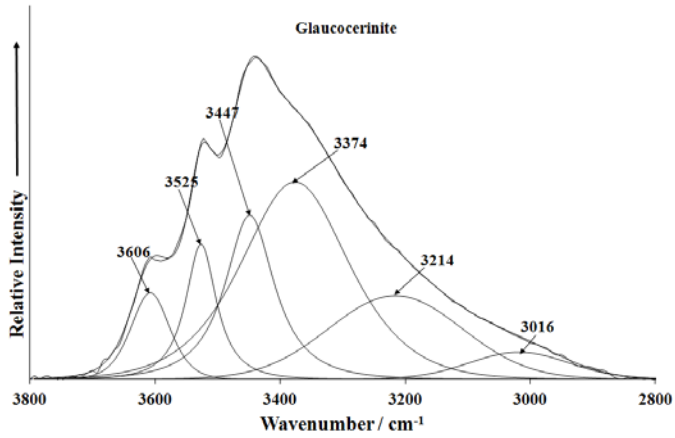

Figure 4a Raman spectrum of glaucocerinite (upper spectrum) in the 2600 to 3800 cm^{-1} spectral range and Figure 4b infrared spectrum of glaucocerinite (lower spectrum) in the 2800 to 3800 cm^{-1} spectral range

399

400

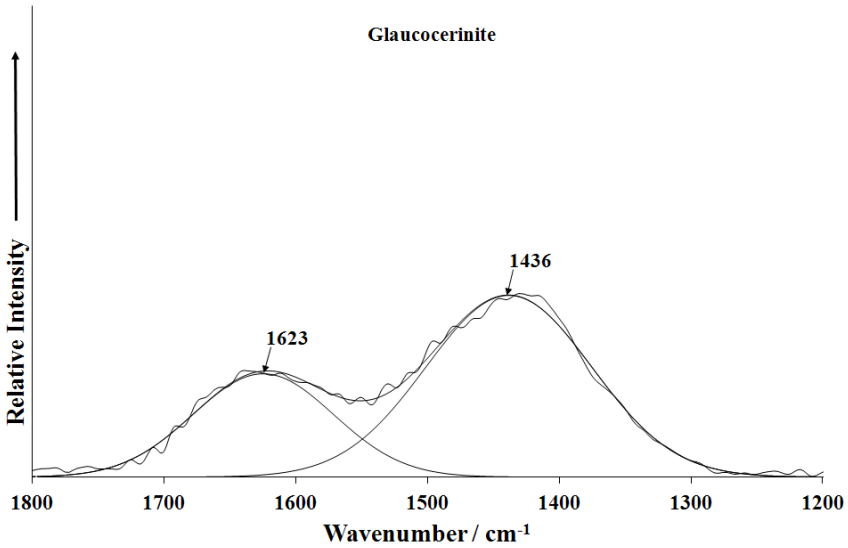

Figure 5 Infrared spectrum of glaucocerinite (lower spectrum) in the 1200 to 1800 cm^{-1} spectral range

401

402

403

404